Data Summary and Concluding Remarks

The experimental data confirm that blunt entry bodies in the terminal regime experience a substantial decrease in their flight stability when they are rolling. From comparisons between the measured angle-of-attack data and the six-degree-of-freedom simulations, it appears that conventional flight analyses based on a symmetric force model can adequately predict the level of angle-of-attack divergence (or convergence) in this regime. It does not, however, describe or explain the oscillatory perturbations that were observed during most of the drops, and the data are not of high enough quality to accurately describe the perturbations or draw any conclusions about them. With this qualification, the following observations are made from the data summary in Fig. 8: 1) the effective dynamic stability coefficient tends to increase (in a favorable way) as the body roll rate increases; 2) the sharper configurations (smaller cone angles) are more stable than the blunter configurations; and 3) configurations with round trailing edges are slightly less stable than their sharp-edged counterparts.

For anyone contemplating performing similar tests I would suggest that internal instrumentation be considered as an alternative method of obtaining data. The photographic method was convenient and relatively inexpensive, but the quality of the data was not satisfactory for a detailed analysis. Since the models can be recovered undamaged, a gyro-telemetry system might be used.

References

[1] Shirley, D. H. and Misselhorn, J. E., "Instability of High-Drag Planetary Entry Vehicles at Subsonic Speeds," *Journal of Spacecraft and Rockets*, Vol. 5, No. 10, Oct. 1968, pp. 1165–1169.

[2] Jaffe, P., "Terminal Dynamics of Atmospheric Entry Capsules," *AIAA Journal*, Vol. 7, No. 6, June 1969, pp. 1157–1158.

[3] Bendura, R. J., "Low Subsonic Static and Dynamic Stability Characteristics of Two Blunt 120° Cone Configurations," TN D-3853, Feb. 1967, NASA.

JUNE 1971 J. SPACECRAFT VOL. 8, NO. 6

Re-Entry Capsule Dynamics

LARS E. ERICSSON* AND J. PETER REDING†
Lockheed Missiles & Space Company, Sunnyvale, Calif.

A bulbous base can have a profound effect on the aerodynamic characteristics of blunt space capsules and slender re-entry bodies and can cause drastic loss of dynamic stability. A careful examination of available experimental data reveals that the often complex effects of bulbous bases can be explained using quasi-steady separated flow concepts. In general, a bulbous base adversely affects the vehicle dynamics but increases the static stability.

Nomenclature

A_F = forebody axial force, kg; coefficient $C_{AF} = A_F/q_0S$
c = reference length, m (usually $c = d$)
d = body caliber, m
M = Mach number
M_A = axial force pitching moment, kg-m; coefficient, $C_{m_A} = M_A/q_0Sc$
N = normal force, kg; coefficient $C_N = N/q_0S$
q = pitch rate, rad/sec; $q = \dot{\theta}$
q_0 = freestream dynamic pressure, $\rho U^2/2$
R_c = Reynolds number, based on c
S = reference area, m^2, $S = \pi c^2/4$
T = period of oscillation, sec
$t, \Delta t$ = time, sec
U = freestream velocity, m/sec
$\bar{U}$ = mean convection velocity, m/sec
x = horizontal coordinate, m
$\bar{x}$ = x coordinate of body c.g. or oscillation center
ξ = dimensionless x coordinate from body c.g., $\xi = (x - \bar{x})/c$
z = vertical coordinate, m
α = angle-of-attack, rad or deg; α_0 = trim value
$\tilde{\alpha}$ = local cross-flow angle, rad or deg, Eq. (7)
$\bar{\alpha}$ = angle-of-attack envelope, rad or deg
ρ = air density, kg-sec^2/m^4
ω = oscillation frequency, rad/sec; $\bar{\omega} = \omega c/U$
θ = body attitude perturbation, rad or deg

Subscripts

a, s = attached- and separated-flow, respectively
N = nose
0 = initial or unperturbed value

Superscript

i = induced, e.g., $\Delta^i C_N$ = separation-induced normal force coefficient

Differential symbols

$\dot{\theta}(t)$ = $\partial\theta/\partial t$; $\ddot{\theta}(t) = \partial^2\theta/\partial t^2$; $C_{N\alpha} = \partial C_N/\partial\alpha$; $C_{m_\theta} = (\partial C_m/\partial\theta)_{\theta=0}$; $C_{m_q} + C_{m_{\dot{\alpha}}} = C_{m_{\dot{\theta}}} = [\partial C_m/\partial(c\dot{\theta}/U)]_{\theta=0}$; $C_{m_{\dot{q}}} = [\partial C_m/\partial(c\dot{q}/U^2)]_{\theta=0}$

Integrated quantities

$C_{\bar{m}_\theta}$; $C_{\bar{m}_{\dot{\theta}}}$ = defined in Eqs. (18) and (17), respectively

Presented as Paper 70-563 at the AIAA Atmospheric Flight Mechanics Conference, Tullahoma, Tenn., May 13–15, 1970; submitted June 16, 1970; revision received January 13, 1971. The flow concepts used in the paper were developed in studies for NASA under Contracts NAS 8-5338, NAS 8-11238, and NAS 1-6450.

* Senior Staff Engineer. Associate Fellow AIAA.
† Research Specialist. Member AIAA.

Introduction

BULBOUS bases are rather common on modern re-entry vehicles. Manned re-entry capsules usually comprise a blunt heat shield in the wake of which the valuable payload is shielded and supposedly hidden from a hostile environment. On the more slender re-entry configurations used for military applications, convex rounded bases are used for other equally compelling reasons. Although the bulbous base in some cases may have little effect on the static characteristics, it can have drastic effects on the vehicle dynamics, causing un-

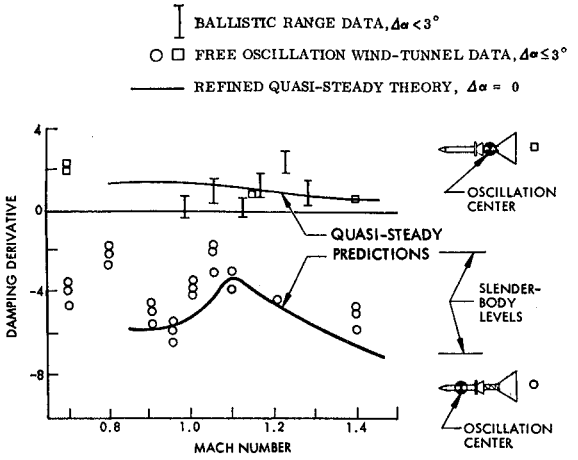

Fig. 1 Dynamic characteristics of the Apollo-Saturn escape system.

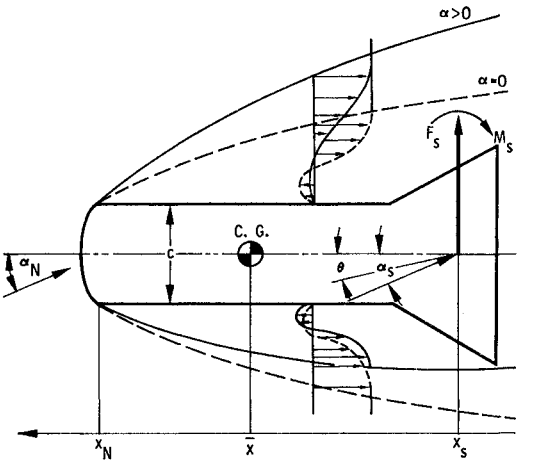

Fig. 3 Nose-induced separation.

damping in pitch[1,2] and a flight behavior characterized by circular limit-cycle oscillations.[3]

When the forebody is very blunt, the flow that separates off the shoulder will eventually reattach on the trailing payload shroud, if the Mach number is high enough, and will generate aerodynamic loads that often result in dynamic instability. If the near wake is formed by flow separation off a rounded base, the associated aerodynamics often lead to dynamic instability at transonic and subsonic Mach numbers. Both of these flow phenomena, which in some cases even occur simultaneously, will be discussed in detail, based on available experimental data, and analytical relationships between dynamic and static characteristics will be developed.

Flow Reattachment Effects

The Apollo-Saturn escape configuration provides a good example of flow reattachment effects (Fig. 1). The quasi-steady estimate,[4] which predicts the dynamic instability rather well, was obtained as follows: Consider the deeply "hammerheaded" geometry sketched in Fig. 2. The loads (F_s, M_{A_s}) on the body submerged in the wake from the blunt nose are dependent upon the relative wake deflection Δz as well as on local angle-of-attack α_s. That is,

$$F_s = q_0 S[(\partial C_{N_s}/\partial z)\Delta z + (\partial C_{N_s}/\partial \alpha_s)\alpha_s] \qquad (1)‡$$

The wake movement Δz is caused not only by the actual relative deflection, $-(z_N - z_s)$, but also by the directing effect that the nose, the wake source, has on the wake. If the nose angle-of-attack is α_N, the total wake deflection Δz may be expressed as follows in linearized form §

$$\Delta z = -(z_N - z_s) + (\partial \Delta z/\partial \alpha_N)\alpha_N \qquad (2)$$

Thus, F_s becomes

$$F_s = q_0 S[(\partial C_{N_s}/\partial \alpha_N)\alpha_N - (\partial C_{N_s}/\partial z)(z_N - z_s) + (\partial C_{N_s}/\partial \alpha_s)\alpha_s] \qquad (3)$$

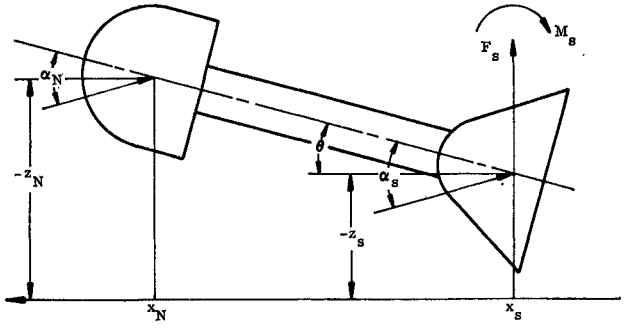

Fig. 2 Forebody wake-generating geometry.

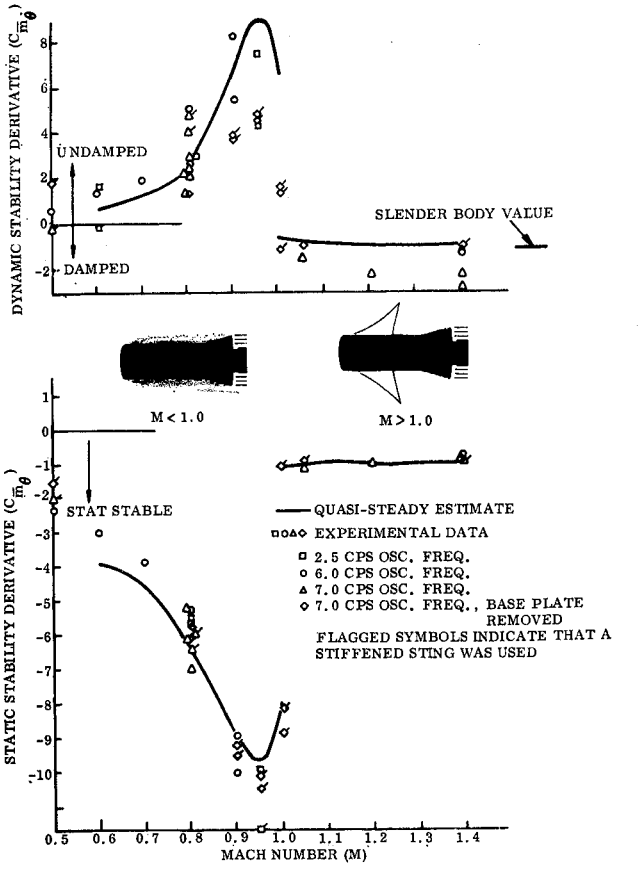

Fig. 4 Oscillatory derivatives of a blunt cylinder-flare body for 1.0° amplitude oscillations around $\alpha_0 = 0$.

‡ Likewise, the moment M_{A_s} due to the axial force couple is

$$M_{A_s} = q_0 Sc[(\partial C_{m_{A_s}}/\partial z)\Delta z + (\partial C_{m_{A_s}}/\partial \alpha_s)\alpha_s]$$

§ Finite amplitude data are obtained through integration, as shown later.

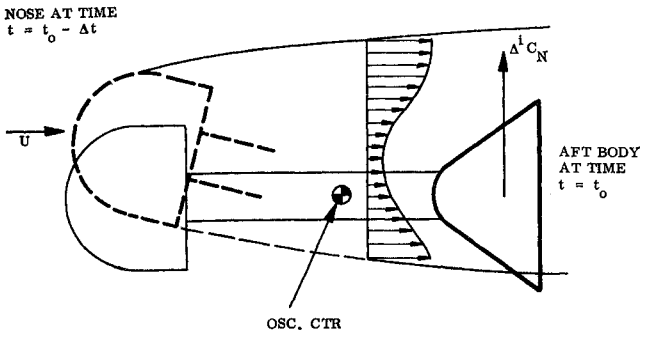

Fig. 5 Dynamic effect of time lag.

where

$$\partial C_{N_s}/\partial\alpha_N = (\partial C_{N_s}/\partial z)(\partial z/\partial\alpha_N)$$

For a nondirecting wake source, such as the flow separation disk on the escape rocket in Fig. 1, the nose-directing effect is zero, $\partial C_{N_s}/\partial\alpha_N = 0$. A blunt nose, as sketched in Fig. 2, will direct the wake upward, producing $\partial C_{N_s}/\partial\alpha_N > 0$, whereas a slender wake source will direct it downward, $\partial C_{N_s}/\partial\alpha_N < 0$, as verified by experiments.[5] If the wake source support is made increasingly larger in diameter, it starts to direct the wake (and, accordingly, experiences aerodynamic loads). Finally, when the support and nose diameters are of the same size, the effect of relative wake deflection disappears, $\partial C_{N_s}/\partial z = 0$. The center of the wake no longer moves, but the wake boundaries do, and the flow geometry sketched in Fig. 3 can be visualized for the so-called nose-induced separation.[5] The wake directing effect of α_N still exists but is no longer accomplished by a translatory wake displacement, as was the case for the free wake; it is produced through a movement of the wake boundaries, resulting in a compression of the windward side and stretching of the leeward side shear flow profiles. That is, α_N still induces a force on the flare

$$F_s = q_0 S[(\partial C_{N_s}/\partial\alpha_N)\alpha_N + (\partial C_{N_s}/\partial\alpha_s)\alpha_s] \qquad (4)$$

In the nonsteady case, the α_N-time-history has to be considered. In a quasi-steady approximation, the time-history effects are represented in lumped form by the nose attitude at a discrete time increment Δt earlier than the present time. Thus,

$$F_s(t) = q_0 S[(\partial C_{N_s}/\partial\alpha_N)\alpha_N(t - \Delta t) + (\partial C_{N_s}/\partial\alpha_s)\alpha_s(t)] \qquad (5)$$

Δt is the time required for the force F_s to respond to changes in the nose cross-flow angle α_N. This time lag Δt is estimated using the average downstream convection speed $\bar{U}$ in the separated flow wake

$$\Delta t = (x_N - x_s)/\bar{U}: \quad \bar{U}/U = (C_{AF_s}/C_{AF_a})^{1/2} \qquad (6)$$

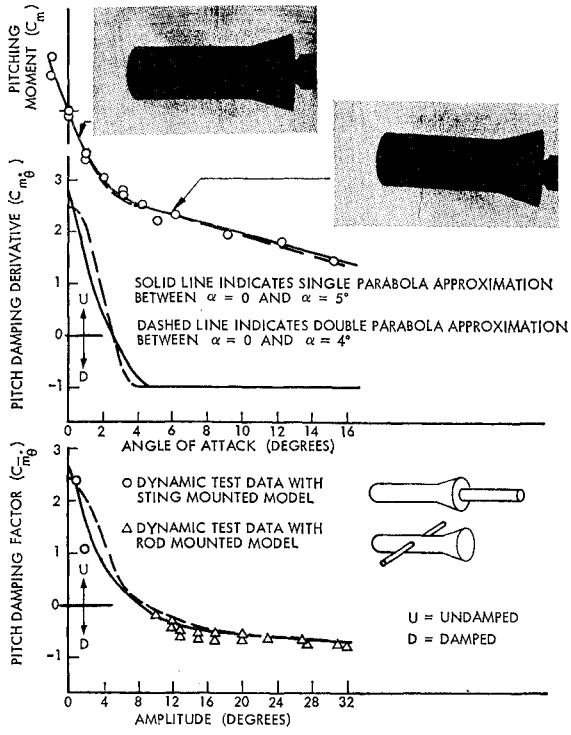

Fig. 6 Aerodynamic characteristics of a blunt cylinder-flare body with nose-induced separation at $M = 0.9$.

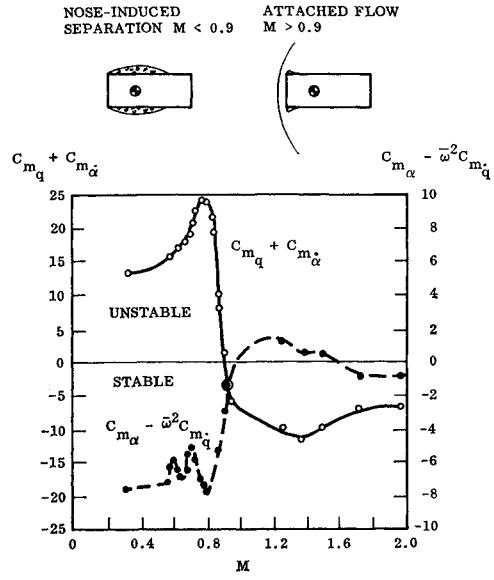

Fig. 7 Dynamic characteristics of flat canister at $\alpha_0 = 0$ and $\Delta\theta = 1.5°$.

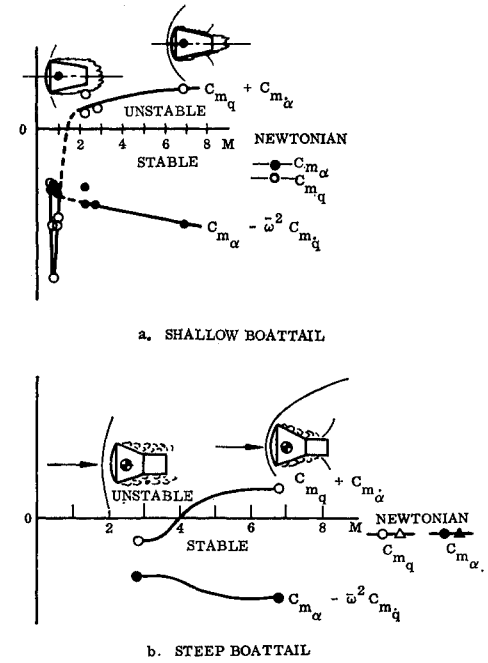

Fig. 8 Dynamic characteristics of blunt re-entry capsule at $\alpha_0 = 0$ and $\Delta\theta = 2°$.

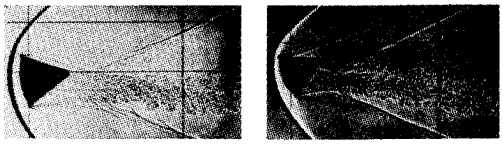

Fig. 9 Flowfield over Apollo-like capsule at $M = 4.0$.

where $C_{A_{F_s}}$ and $C_{A_{F_a}}$ are the flare forebody axial forces in separated and attached flow, respectively. This gives a slightly high[¶] value of Δt, since the reverse flow region is neglected. The difference, however, should be small except for the critical geometry. In the latter case the reverse flow region is large and upstream communication effects from the flare would also have to be included.[6] That is, as long as the dynamic effects of flow separation can be modeled mathematically as shown here, Eq. (6) will give a sufficiently good estimate of Δt.

The effective cross-flow angle $\tilde{\alpha}$ is

$$\tilde{\alpha} = \alpha_0 + \theta + \dot{z}/U \tag{7}$$

Thus, for oscillations around a fixed c.g. (Fig. 3),

$$\alpha_s(t) = \alpha_0 + \theta(t) - \xi_s[c\dot{\theta}(t)/U] \tag{8a}$$

$$\alpha_N(t - \Delta t) = \alpha_0 + \theta(t - \Delta t) - \xi_N[c\dot{\theta}(t - \Delta t)/U] \tag{8b}$$

For the slow oscillations, $\bar{\omega}^2 \ll 1$, which are of practical interest for rigid body oscillations at transonic and supersonic speeds,

$$\theta(t - \Delta t) = \theta(t) - \Delta t\dot{\theta}(t) \ldots \approx \theta - \Delta t\dot{\theta} \tag{9a}$$

$$\theta(t - \Delta t) = \theta(t) - \Delta t\dot{\theta}(t) \ldots \approx \dot{\theta} \tag{9b}$$

Thus,

$$\alpha_s(t) \approx \alpha_0 + \theta - \xi_s(c\dot{\theta}/U) \tag{10a}$$

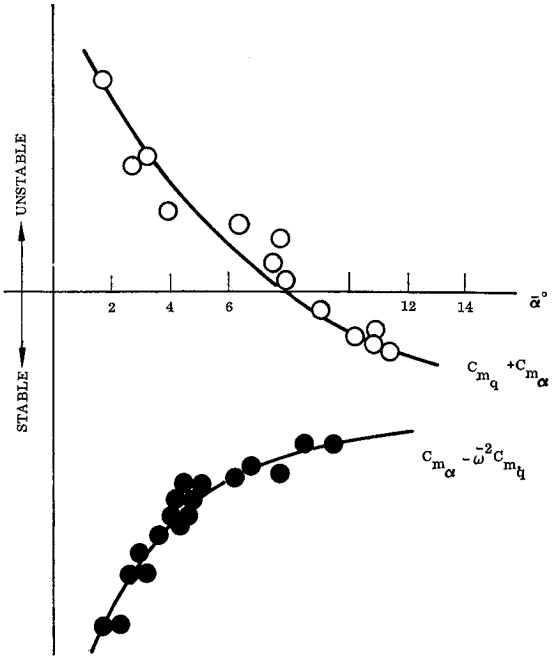

Fig. 10 Ballistic range data for a slender cone with rounded base at $M \approx 0.6$.

¶ This usually means overestimating the undamping, i.e., a conservative value. At high M, the assumption of constant density through the wake would not be permissible.

$$\alpha_N(t - \Delta t) \approx \alpha_0 + \theta - (U\Delta t/c + \xi_N)c\dot{\theta}/U \tag{10b}$$

and Eq. (5) becomes

$$F_s(t) = q_0 S C_{N_s}(t) \tag{11a}$$

$$C_{N_s}(t) = (\partial C_{N_s}/\partial\alpha_s)[\alpha_0 + \theta - \xi_s(c\dot{\theta}/U)] + \partial C_{N_s}/\partial\alpha_N[\alpha_0 + \theta - (U\Delta t/c + \xi_N)c\dot{\theta}/U] \tag{11b}$$

$C_{N_s}(t)$ may be rearranged as

$$C_{N_s}(t) = (C_{N\alpha_s} + \Delta^i C_{N\alpha_s})(\alpha_0 + \theta) - \left[\xi_s C_{N\alpha_s} + \left(\xi_N + \frac{U\Delta t}{c}\right)\Delta^i C_{N\alpha_s}\right]\frac{c\dot{\theta}}{U} \tag{12}$$

where $\Delta t = c(\xi_N - \xi_s)/\bar{U}$; $C_{N\alpha_s} = \partial C_{N_s}/\partial\alpha s$; and $\Delta^i C_{N\alpha_s} = \partial C_{N_s}/\partial\alpha_N$. Thus, for slow oscillations of infinitesimal amplitude ($|\theta| \ll 1$)

$$\partial C_{N_s}/\partial\theta = C_{N\theta_s} = C_{N\alpha_s} + \Delta^i C_{N\alpha_s} \tag{13}$$

$$\partial C_{N_s}/\partial(c\dot{\theta}/U) = C_{N\dot{\theta}_s} = -\xi_s C_{N\alpha_s} - [(U/\bar{U})(\xi_N - \xi_s) + \xi_N]\Delta^i C_{N\alpha_s} \tag{14}$$

where $C_{N\theta_s}$ is the total derivative measured in static tests. Using the average velocity (and dynamic pressure) concept of Eq. (6),

$$C_{N\alpha_s} = (C_{A_s}/C_{A_a})C_{N\alpha_a} \tag{15}$$

where $C_{N\alpha_a}$ is the flare force in attached flow. The remainder of the force derivative measured in the static test is $\Delta^i C_{N\alpha_s}$.

Using static experimental data in this manner to define $C_{N\alpha_s}$ and $\Delta^i C_{N\alpha_s}$, as well at Δt in Eq. (6), the pitch damping derivative for infinitesimal amplitude oscillations was computed and compared with experimental dynamic data for 1° amplitude oscillations (Fig. 4). The undamping resulting from the nose-induced separation at subsonic speeds is remarkably well predicted. A typical characteristic of the effects of separated flow, at least for the low reduced frequencies for which quasi-steady treatment is applicable, is the opposite effects on dynamic and static stability. Nose-induced separation causes a large increase in static stability, but causes dynamic instability. The sketch in Fig. 5 illustrates how this is the natural result of the convective time lag associated with the separation-induced force $\Delta^i C_N$.

When the flare comes down to $\alpha = 0$ at time t, it resides in the separated flow wake generated at an earlier instant $t - \Delta t$. The resulting residual force at $\alpha = 0$ drives the pitch rotation and, hence, is dynamically destabilizing or undamping. Statically, of course, the force $\Delta^i C_N$ is stabilizing.

Since the aerodynamic characteristics are highly nonlinear, the damping derivative $C_{m\dot{\theta}}$ loses meaning when the oscillation amplitudes are no longer small. One can define an effective damping derivative $C_{\bar{m}\dot{\theta}}$ which is the (false) linear measure $C_{m_q} + C_{m_{\dot{\alpha}}}$ of the energy dissipation per cycle in dynamic wind-tunnel experiments

$$C_{\bar{m}\dot{\theta}} = \int_{t_0}^{t_0+T} C_m d\theta \Big/ \frac{c}{U}\int_{t_0}^{t_0+T} (\dot{\theta})^2 dt \tag{16}$$

For harmonic oscillations, $\theta = \Delta\theta \sin\omega t$, Eq. (16) becomes

$$C_{\bar{m}\dot{\theta}} = \frac{1}{\pi\Delta\theta}\frac{1}{\bar{\omega}}\int_{\omega t_0}^{\omega t_0+2\pi} C_m \cos(\omega t) d(\omega t) \tag{17}$$

Similarly, the effective stability derivative $C_{\bar{m}\theta}$, the linear measure of aerodynamic stiffness extracted from dynamic

wind tunnel test data, can be defined as

$$C_{\bar{m}\theta} = \frac{2}{[(\alpha_{max})^3/|\alpha_{max}|] - [(\alpha_{min})^3/|\alpha_{min}|]} \times \left\{ \frac{\alpha_{max}}{|\alpha_{max}|} \int_0^{|\alpha_{max}|} C_m d\alpha - \frac{\alpha_{min}}{|\alpha_{min}|} \int_0^{|\alpha_{min}|} C_m d\alpha \right\} \quad (18)$$

where $\alpha_{max} = \alpha_0 + \Delta\theta$, and $\alpha_{min} = \alpha_0 - \Delta\theta, |\alpha_0| < \Delta\theta$.

In Fig. 6 the top graph shows the nonlinear $C_m(\alpha)$ associated with the nose-induced separation. The middle graph shows how the infinitesimal amplitude oscillations become undamped for trim angles below $\alpha_0 = 3°$. The two different fairings to the static data give slightly different $C_{m\dot{\theta}}$ variation with α. The bottom graph shows how the effective damping derivative $C_{\bar{m}\dot{\theta}}$ varies with amplitude for oscillations around $\alpha_0 = 0$. Again, the agreement between the quasi-steady predictions and the dynamic test data is remarkably good. The data show that planar oscillations will diverge or converge to a limit cycle amplitude of ~8°.

Even without a flare the nose-induced separation generates aft body loads. Figure 7 shows how the dynamic characteristics of a cylindrical canister[7] are very similar to those of a blunt-nosed cylinder-flare body (Fig. 4). If the aft body is boat-tailed, as is often the case for re-entry capsules, the aft body flow reattachment effects are not realized until M reaches supersonic values, but then the typical statically stabilizing and dynamically destabilizing trends are again realized.[8] If the boat-tail is shallow, the reattachment occurs at a lower M (Fig. 8a) than when it is steep (Fig. 8b). On a Mercury capsule this reattachment is observed at M = 3, resulting in oscillations that diverge to more than 20° limit cycle amplitude.[9] Even the very steep boat-tail on an Apollo-like re-entry capsule experiences flow reattachment if the Mach number is high enough[10] (Fig. 9). The reattaching flow generates the same highly nonlinear characteristics in re-entry capsules as on flared bodies.

Flow Separation Effects

The geometries discussed so far have had blunt forebodies, and the dynamically destabilizing effect was caused by the time lag occurring before a change at the wake source, i.e., the forebody, has been communicated downstream to affect the flow reattachment on the aft body. When the forebody is slender, the characteristics are similar to those discussed earlier; thus, the large increase in static stability at lower amplitudes is accompanied by an even greater decrease of dynamic stability, (Fig. 10), resulting in limit cycle oscillations.[3,10] Wind-tunnel data[1,11] illustrate further that the undamping is caused by the base roundness.

The lift developed over the forebody initially directs the wake downward. As the wake is turned back into the free-stream direction, a transverse pressure gradient is established to accomplish the turning of the wake. This difference in windward- to leeward-side recompression pressures, and associated differences in the back flow velocities in the recirculatory region, generate the positive aft body force. The shadowgraph and flow sketch in Fig. 11** not only substantiate that the windward side wake-recompression shock is strengthened, but also show that it is closer to the base than on the leeward side, thus facilitating the windward-side upstream communication dominance. At subsonic speeds, shoulder roundness permits the near-wake effects to be propagated upstream of the base with a resulting increase of static and degradation of dynamic stability (Fig. 12).

It is obvious that a time lag will occur before a change in forebody lift has resulted in a near-wake flow modification and corresponding aft body force generation. Thus, the

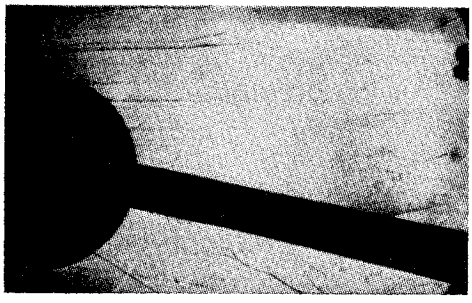

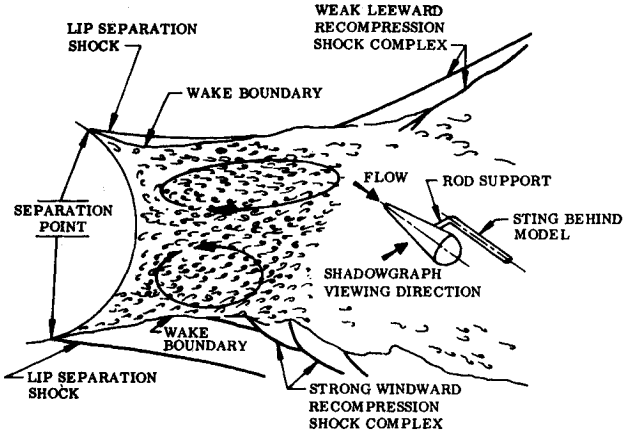

Fig. 11 Near wake flow patterns of a slender cone with rounded base at M = 2.0 and α_0 = 12°.

near-wake effect causes increased static and decreased dynamic stability, just as the flow reattachment effects discussed earlier. Figure 13 shows how the measured base-roundness-induced degradation of dynamic stability correlates with the forebody lift derivative at subsonic speeds where the near-wake effect is realized.††

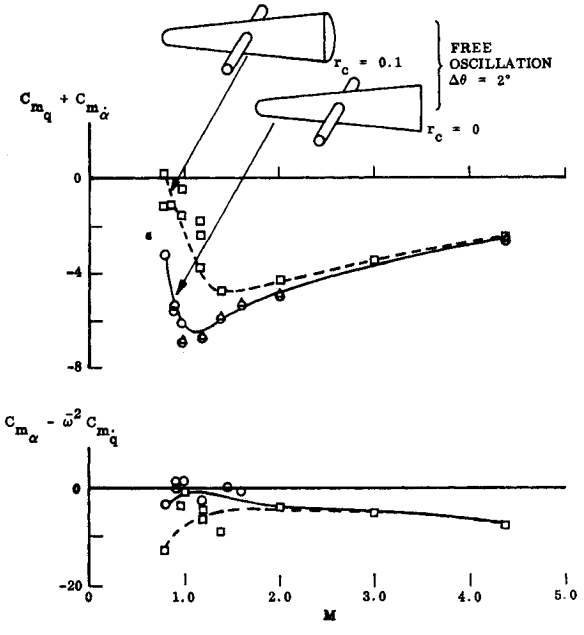

Fig. 12 Effect of base shoulder radius on oscillatory derivatives of a slender cone with a large bulbous base.

** The flow sketch in Fig. 11 shows the salient flowfield characteristics free of the extraneous out-of-plane sting effects (see inset sketch).

†† The undamping can be due only to a forebody load modification,[2] since the dome itself cannot induce a pitching moment (inset in Fig. 13). Base-roundness serves to enhance the wake effect on the forebody by facilitating communication with the wake. At supersonic speeds the communication from the near wake upstream of the rounded base can occur only through the subsonic portion of the boundary layer, and the effects are small.

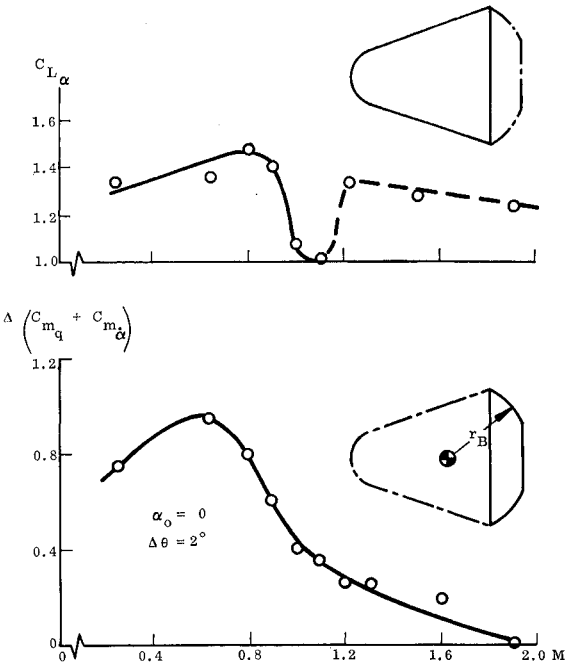

Fig. 13 Correlation of bulbous base effect with forebody lift.

If the forebody is so blunt as to have a negative lift derivative, the wake is inclined opposite to the angle of attack[12] (Fig. 9), and the effect of the bulbous base is reversed; i.e., it is dynamically damping rather than undamping. This has indeed been observed experimentally.[13]

Thus, both the flow reattachment and near-wake effects can by themselves cause dynamic instability. Figure 14 gives an example of how the adverse effects can be compounded.[2] At transonic speeds, $0.9 < M < 1.2$, the blunt nose causes flow separation‡‡ with attendant reattachment-induced degradation of dynamic stability (and increase of static stability). The boattail causes undamping near-wake effects that persist throughout the subsonic and transonic speed region.

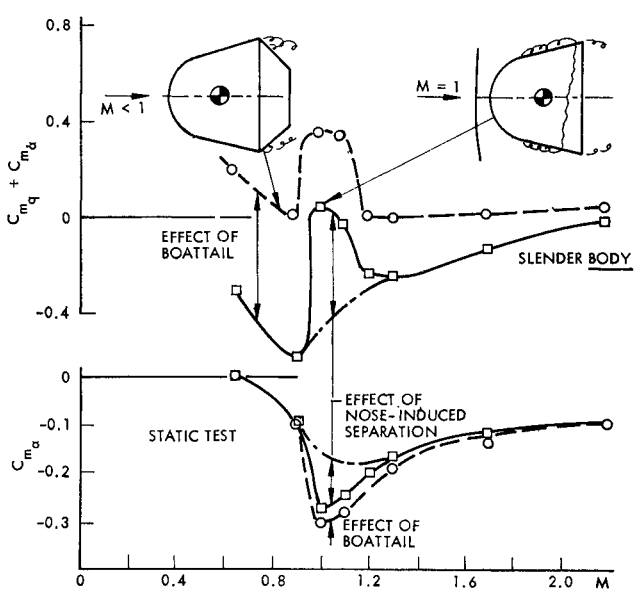

Fig. 14 Pitch damping and static stability of a blunt cone with and without boat-tail.

‡‡ It is doubtful that the boundary layer would separate at $\alpha = 0$ unless it were laminar.

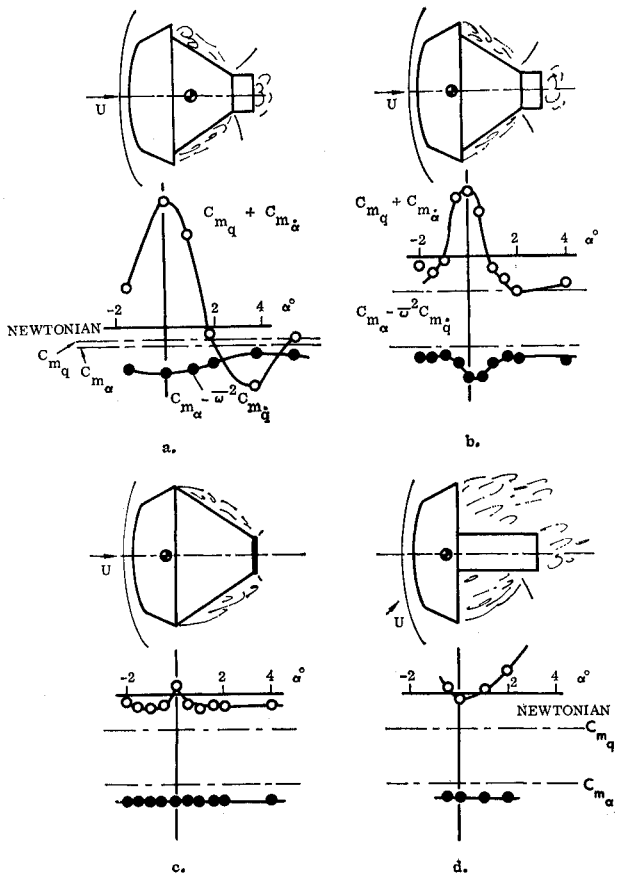

Fig. 15 Re-entry capsule damping at $M = 2.5$ and $\Delta\theta = 1.5°$.

Effects of Modifications and Fixes

It is clear from what has just been said that the dynamic instability caused by flow reattachment aft of a very blunt forebody can be eliminated or greatly reduced by going to a rounded or dome-shaped base. However, this would mean less separated flow and consequently increased heat shield requirements.

The adverse dynamic effects of flow reattachment decrease when the center of gravity is moved forward[14] (Figs. 15a and

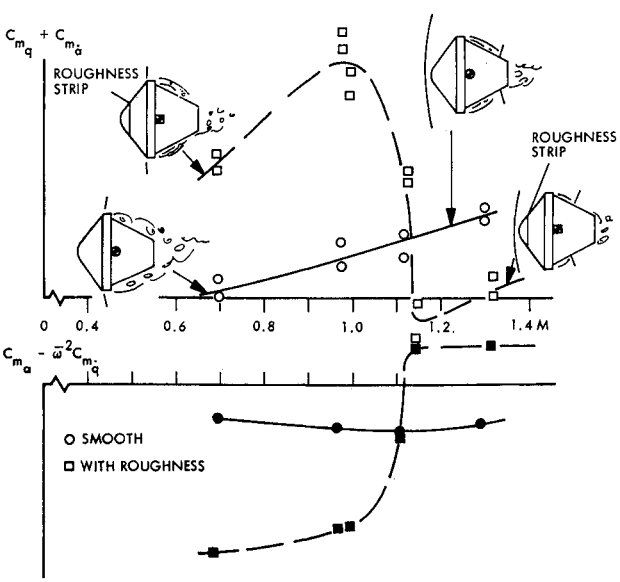

Fig. 16 Effect of roughness on re-entry capsule dynamics at $\alpha_0 = 0$, $\Delta\theta = 2°$, and $2.0 \times 10^6 < R_c < 2.7 \times 10^6$.

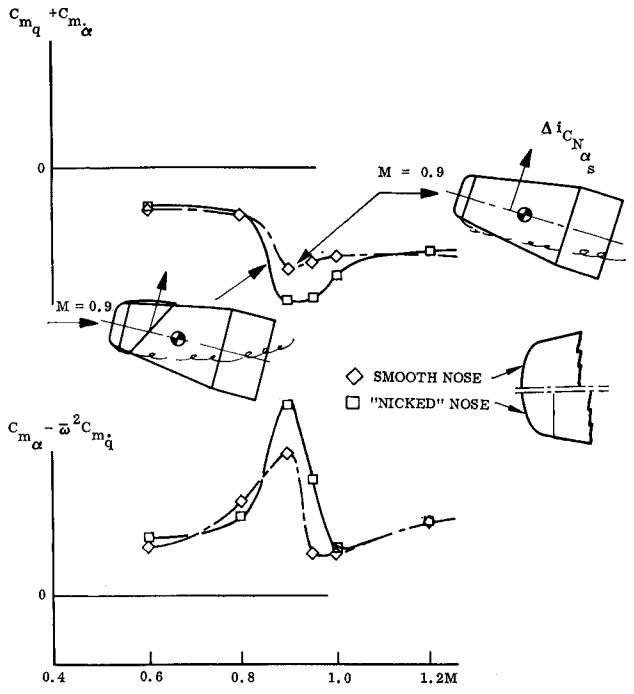

Fig. 17 Oscillatory derivatives of a blunt cone-cylinder for 2° amplitude oscillations at $\alpha_0 = 0$.

15b). Equation (14) reveals the reason for this effect. When c.g. is aft of the shoulder, ξ_N is positive and adds to the magnitude of the bracket, the dynamic amplifier of $\Delta^i C_{N\alpha}$ in Eq. (14). When c.g. is moved forward of the shoulder, ξ_N becomes negative and the dynamic amplification is decreased (ξ_s is negative in both cases—see insets in Figs. 15a and 15b). Comparing the static ($C_{m\alpha}$) and dynamic ($C_{m_q} + C_{m_{\dot\alpha}}$) nonlinearities in Figs. 15a and 15b, one can see that the dynamic amplification more than makes up for the decrease in moment lever arm ($-\xi_s$). The separation-induced undamping effect increases in spite of the lesser static stability effect for the aft c.g. The Apollo escape system exhibited the same effect of moving the c.g. forward of the wake generator (Fig. 1). In that case, the movement was large enough to eliminate the undamping effect (the bracket in Eq. (14) was near zero, i.e., $\xi_s \approx 2\xi_N$). Physical restraints make this magnitude c.g. movement impossible for the re-entry capsules (Figs. 15a and 15b).

By removing most of the reattachment-inviting cylindrical tail-end, as well as the step-down shoulder and associated larger wake turning, the reattachment effects can be greatly reduced (Fig. 15c). They will, of course, reappear in force again if the Mach number is increased sufficiently. Figure 15d illustrates that the problem may be eliminated at $\alpha = 0$ only to reappear at angle-of-attack. The nonlinear characteristics caused by sudden reattachment on re-entry capsules or sudden separation on blunt cylinder-flare bodies[15] are not considered in the present paper.

Figures 15b–15d show that the aft body modifications had little effect on static stability. The large dynamic effects are caused by the large "effective"§§ time lags involved. Figure 16 illustrates accidentally how subtle changes of the forebody geometry can have dramatic effects on capsule dynamics.[16] The roughness trip improved the forebody boundary layer enough to cause wake reattachment on the aft body at subsonic speeds. At supersonic speeds, where also the no-trip configuration has wake reattachment, the trip causes earlier reattachment with correspondingly decreased separation-induced effects.

§§ So-called accelerated flow effects[17] are adding to the delays due to convective time lag.

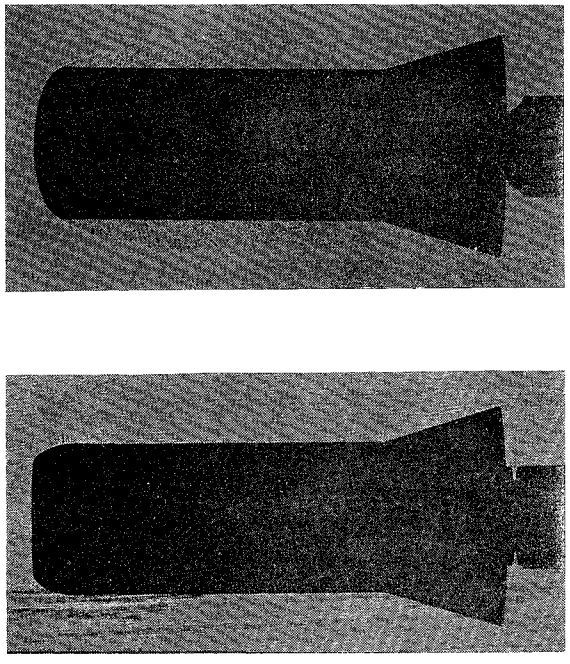

Fig. 18 Effect of subtle modification of nose geometry on nose-induced separation.

When nose-induced separation and reattachment all occur forward of the c.g. the effects on the dynamic stability are beneficial (Fig. 17), as can be expected (both ξ_s and ξ_N are positive in Eq. (14); and $\Delta^i C_{N\alpha_s} \gg C_{N\alpha_s}$). The associated large decrease of static stability confirms that the time lag effects are small, and that the reattachment is not taking place near the aft cone-cylinder shoulder.¶¶ In that case, the beneficial dynamic effects would have been much larger (relative to the static stability effects). The "nicked-down" nose has shorter separation bubble and consequently increased damping. Using biconic nose shapes, or the blunt face-rounded nose geometry shown in Fig. 18, can reduce the nose-induced separation greatly and even completely eliminate it. This is due to the "preseparation" which generates a reattaching strong boundary layer before the critical last nose shoulder.[17]

The rounded-base-shoulder effect can be minimized if flow fences or other devices are used to hinder the reverse flow communication over the shoulder, (Fig. 19).[1] It can

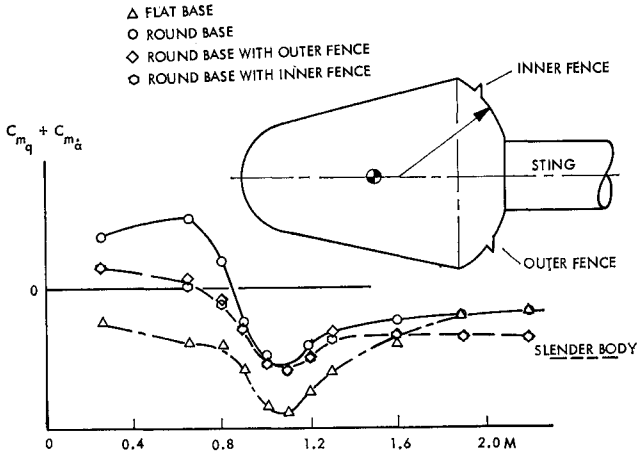

Fig 19 Effect of changes in base contour on cone pitch damping at $\alpha_0 = 0$ and $\Delta\theta = 1.5°$.

¶¶ Where the reattaching flow would generate a negative load.[21]

hardly be expected that the data in Fig. 19 represent the ultimate in what could be accomplished in reducing or eliminating the undamping effect of base roundness. A "forebody overhang" over the base dome are but one of many configuration modifications that could be tried.

From the description of the flow mechanism associated with the rounded-base-shoulder effect, it is obvious that the sting support will have a large influence on the measured data.[8,11] The dynamic sting interference from a cylindrical sting is damping,[18,19] and as a consequence the undamping effect of a rounded-base-shoulder measured in a wind-tunnel test will be substantially less than that realized in free flight. If boundary-layer transition occurs on the aft body, additional complications arise.[20] However, all the data used here to illustrate the rounded-base-shoulder effect have been selected in such manner that support interference did not distort the general data trends.

Conclusions

The anomalous dynamic behavior of re-entry capsules is caused by separating and reattaching flows. The separation-induced loads have opposite effects on static and dynamic stability, i.e., statically stabilizing and dynamically destabilizing or undamping, and vice versa. This reversal is the result of the finite time lag in the separated flowfield response to body cross-flow perturbations. A careful analysis of existing experimental data using quasi-steady flow concepts reveals the following: 1) bulbous bases can degrade dynamic stability and often cause undamped oscillations; 2) the undamping is highly nonlinear and usually limited to small angles-of-attack and amplitudes; 3) on a blunt re-entry capsule, undamping results when the wake from the blunt forebody heat shield starts to reattach on the boat-tailed aft body; 4) on slender forebodies with smooth bulbous bases, undamping is realized through upstream communication effects from the wake recompression region. These effects are usually important only at subsonic and transonic speeds, although they will recur for high-speed low-density flows; 5) if the forebody is blunt (i.e., with negative lift derivative), the effect of the smooth bulbous base is to enhance dynamic stability; 6) the undamping is very sensitive to subtle geometry changes, and the adverse dynamic effects can be reduced greatly through redesign defined by use of quasi-steady flow concepts.

References

[1] Wehrend, W. R., Jr., "A Wind-Tunnel Investigation of the Effect of Changes in Base Contour on the Damping in Pitch of a Blunted Cone," TN D-2062, 1963, NASA.

[2] Wehrend, W. R., Jr., "Wind Tunnel Investigation of the Static and Dynamic Stability Characteristics of a 10° Semi-vertex Angle Blunted Cone," TN D-1202, 1967, NASA.

[3] Murphy, C. H., "Nonlinear Analysis of Free Flight Motion," Paper 10, Vol. 1 *Transactions of the Second Technical Work Shop on Dynamic Stability Testing,* Arnold Engineering Development Center, Arnold Air Force Station, Tenn., April 20–22, 1965.

[4] Ericsson, L. E. and Reding, J. P., "Aeroelastic Characteristics of Saturn 1B and Saturn V Launch Vehicles," LMSC-M-37-5, Contract NAS 8-11238, 1967, Lockheed Missiles & Space Co., Sunnyvale, Calif.

[5] Ericsson, L. E. and Reding, J. P., "Dynamics of Separated Flow Over Blunt Bodies," LMSC 2-80-65-1, Contract NAS 8-5338, Dec. 1965, Lockheed Missiles & Space Co., Sunnyvale, Calif.

[6] Ericsson, L. E., Reding, J. P., and Guenther, R. A., "Effects of Shock-Induced Separation," LMSC L-87-69-1, Contract NAS 8-20354, July 1969, Lockheed Missiles & Space Co., Sunnyvale, Calif.

[7] LaBerge, J. G., "Effect of Flare on the Dynamic and Static Moment Characteristics of a Hemisphere-Cylinder Oscillating in Pitch at Mach Numbers from 0.3 to 2.0," Rept. LR-295, Jan. 1961, National Research Council of Canada.

[8] Ericsson, L. E. and Reding, J. P., "Aerodynamic Effects of Bulbous Bases," CR-1339, 1969, NASA.

[9] Sommer, S. C., Short, B. J., and Compton, D. L., "Free-Flight Measurements of Static and Dynamic Stability of Models of the Project Mercury Re-entry Capsule at Mach Numbers 3 and 9.5," TM X-373, 1960, NASA.

[10] MacAllister, L. C., "Some Instability Problems with Re-entry Shapes," Memo Rept. 1224, Aug. 1959, Ballistic Research Lab., Aberdeen Testing Grounds, Md.

[11] Wehrend, W. R., Jr., "An Experimental Evaluation of Aerodynamic Damping Moments of Cones with Different Centers of Rotation," TN D-1768, 1963, NASA.

[12] Kruse, R. L., "Transition and Flow Reattachment Behind an Apollo-Like Body at Mach Numbers to 9," TN D-4645, 1968, NASA.

[13] Sammonds, R. I., "Transonic Static and Dynamic Stability Characteristics of Two Large Angle Spherically Blunted High Drag Cones," AIAA Paper 70-564, Tullahoma, Tenn., 1970.

[14] Beam, B. H. and Hedstrom, C. E., "The Damping in Pitch of Bluff Bodies of Revolution at Mach Numbers from 2.5 to 3.5," TMX-20, 1959, NASA.

[15] Ericsson, L. E. and Reding, J. P., "Dynamic Stability Problems Associated with Flare Stabilizers and Flap Controls," *Journal of Spacecraft and Rockets,* Vol. 7, No. 2, Feb. 1970, pp. 132–137.

[16] Wiley, H. G., Kilgore, R. A., and Hillje, E. R., "Dynamic Directional Stability Characteristics for a Group of Blunt Re-entry Bodies at Transonic Speeds," TMX-337, 1960, NASA.

[17] Ericsson, L. E., "Aeroelastic Instability Caused by Slender Payloads," *Journal of Spacecraft and Rockets,* Vol. 4, No. 1, Jan. 1967, pp. 65–73.

[18] Reding, J. P. and Ericsson, L. E., "Dynamic Support Interference on Bulbous Based Configurations," *Transactions of the 3rd Technical Workshop on Dynamic Stability Problems,* Vol. II, Paper 7, NASA Ames Research Center, Moffett Field, Calif., Nov. 4–7, 1968.

[19] Reding, J. P. and Ericsson, L. E., "Dynamic Support Interference—Fact or Fiction," AIAA Paper 71-277, Albuquerque, N. Mex., 1970.

[20] Ericsson, L. E. and Reding, J. P., "Boundary Layer Transition and Dynamic Sting Interference," *AIAA Journal,* Vol. 8, No. 10, Oct. 1970, pp. 1886–1888.

[21] Ericsson, L. E. and Reding, J. P., "Analysis of Flow Separation Effects on the Dynamics of a Large Space Booster," *Journal of Spacecraft and Rockets,* Vol. 2, No. 4, July-Aug. 1965, pp. 481–490.